Restoration of segregated, physiological neuronal connectivity by desynchronizing stimulation

J. Neural Eng. **7** (2010) 056008 (14pp) doi:10.1088/1741-2560/7/5/056008

Restoration of segregated, physiological neuronal connectivity by desynchronizing stimulation

Christian Hauptmann[1] **and Peter A Tass**[1,2]

[1] Institute of Neuroscience and Medicine-Neuromodulation INM-7, Research Center Juelich, 52425 Juelich, Germany
[2] Department of Stereotaxic and Functional Neurosurgery, University Hospital, 50924 Cologne, Germany

Received 20 May 2010
Accepted for publication 23 July 2010
Published 1 September 2010
Online at stacks.iop.org/JNE/7/056008

Abstract
The loss of segregation of neuronal signal processing pathways is an important hypothesis for explaining the origin of functional deficits as associated with Parkinson's disease. Here we use a modeling approach which is utilized to study the influence of deep brain stimulation on the restoration of segregated activity in the target structures. Besides the spontaneous activity of the target network, the model considers a weak sensory input mimicking signal processing tasks, electrical deep brain stimulation delivered through a standard DBS electrode and synaptic plasticity. We demonstrate that the sensory input is capable of inducing a modification of the network structure which results in segregated microcircuits if the network is initialized in the healthy, desynchronized state. Depending on the strength and coverage, the sensory input is capable of restoring the functional sub-circuits even if the network is initialized in the synchronized, pathological state. Weak coordinated reset stimulation, applied to a network featuring a loss of segregation caused by global synchronization, is able to restore the segregated activity and to truncate the pathological, synchronized activity.

1. Introduction

Parkinson's disease (PD) is histologically characterized by a loss of mesencephalic dopamine neurons and clinically by motor symptoms (akinesia, rigidity and tremor) (Deuschl *et al* 2000; Bergman and Deuschl 2007). Since the dopaminergic neurons basically project to the basal ganglia, the effects of this dopamine depletion on the information processing and the related activity of the output structures of the basal ganglia, projecting to the thalamus and cortex, are of primary interest to the understanding of the pathophysiology of PD (Bergman *et al* 1998).

As a consequence of the dopamine depletion, abnormal synchronization processes emerge (Bergman *et al* 1998; Wichmann *et al* 1999; Brown 2003; Brown and Williams 2005). Pathological basal ganglia local field potential (LFP) activity is mainly divided into two major bands, below 8 Hz and from 8 to 30 Hz, whereas the latter one is sub-divided into the α-band (8–13 Hz) and the β-band (14–30 Hz). β-band activity inversely correlates with anti-Parkinsonian medication (Brown *et al* 2001; Levy *et al* 2002; Silberstein *et al* 2003, 2005). The medication-induced reduction of β-band activity correlates with an improvement of akinesia and rigidity, but not with an improvement of tremor (Kühn *et al* 2006). In the *in vivo* MPTP monkey model it has been shown that neurons in different regions of the basal ganglia fire coherently, whereas in the healthy monkey they fire in an uncorrelated manner (Nini *et al* 1995). These two observations might be interdependent. In fact, in the cortex synchrony has the potential to limit the coding abilities of neuronal populations (van Vreeswijk and Sompolinsky 1996; Stevens and Zador 1998; Svirskis and Rinzel 2000; Mazurek and Shadlen 2002).

Medically refractory Parkinson patients are treated with deep brain stimulation (DBS). For this, chronic electrodes are implanted into target structures and high-frequency (HF) pulse trains are applied to counteract the over-activation of the output structures of the basal ganglia (Benabid *et al* 1991). The development of HF DBS was an empirical process, mainly relying on intraoperative observations. HF DBS basically mimics the effect of tissue lesioning and strongly

alters, e.g. suppresses, the neuronal firing in a way that is not yet sufficiently understood (Volkmann 2004). Although HF DBS is the golden standard for the therapy of medically refractory movement disorders, there are still limitations of HF DBS: on the one hand, HF DBS may cause adverse effects like dysarthria, dysesthesia, cerebellar ataxia and memory decline (Volkmann 2004; Rodriguez-Oroz *et al* 2005; Freund 2005). On the other hand, HF DBS may be ineffective or its therapeutic effect may wear off over time (Kumar *et al* 2003; Rodriguez-Oroz *et al* 2005). In addition, there is a relevant rate of non-responders. For instance, 11–15% of PD patients have unsatisfactory outcomes with respect to tremor suppression although their depth electrodes are properly placed (Limousin *et al* 1999). Along with the abnormal synchronized activity, a loss of segregation of functional microcircuits (Bergman *et al* 1998; Pessiglione *et al* 2005) and a reduction in the physiological degrees of freedom of the basal ganglia neurons (Gale *et al* 2009) are discussed.

To specifically counteract the abnormal synchronization processes, stimulation methods were developed by Tass and co-workers that achieve a mild but nevertheless effective desynchronization of pathological neuronal synchronization processes (Tass 1999, 2003; Hauptmann *et al* 2005; Popovych *et al* 2005) (for a review see Tass *et al* (2006)). Coordinated reset (CR) stimulation (Tass 2003) is a particularly robust and calibration-free desynchronizing stimulation technique that leads to a therapeutic synaptic reshaping of neuronal networks. Computationally, it has been shown that the desynchronization-induced decrease of the rate of coincident firing reduces the mean synaptic weight and shifts the network to a healthy model attractor state characterized by desynchronized activity and weak connectivity (Tass and Majtanik 2006; Hauptmann and Tass 2007). Long-lasting desynchronization induced by CR stimulation has been experimentally verified in a rat hippocampal slice rendered epileptic by magnesium withdrawal (Tass *et al* 2009).

In this computational study, we go one step further. We do not only focus on an intrinsically oscillatory network and its stimulation induced changes in dynamics and connectivity. Rather we additionally take into account the impact of the sensory input on the connectivity, especially on sensory input-related clusters. We ask whether stimulation unspecifically erases both pathological and physiologically meaningful connectivity patterns. Or whether there is a possibility of specifically restoring physiological connectivity patterns, while wiping out pathological ones. Stimulation-induced restoration rather than suppression or distortion of input-related connectivity might enable profound therapeutic effects.

2. Mathematical model

Our mathematical model comprises a population of bursting STN neurons interacting with a population of globus pallidum exterior (GPe) neurons (Hauptmann and Tass 2007). The STN neurons receive the excitatory input from the surrounding STN neurons and are recurrently inhibited by the GPe neurons. The recurrent inhibition results in a bursting behavior of the STN neurons as observed experimentally (Nini *et al* 1995; Beurrier *et al* 2002). The used spike generator, a modified Morris–Lecar model (Morris and Lecar 1981), allows us to base our investigation on solid results obtained by theoretical analysis, see e.g. Rinzel and Ermentrout (1989). Using such a simplified model of neuronal dynamics is part of our top-down approach to modeling the complex activity of target areas for deep brain stimulation. This stepwise increase of the model complexity—originating at phase oscillator networks (Tass 1999, 2003; Tass and Majtanik 2006; Hauptmann *et al* 2007) and limit-cycle oscillator networks (Popovych *et al* 2005)—is motivated by the still existing lack of experimental data on the micro-level (e.g. concerning physiological mechanisms and topology).

In dimensionless form, the dynamics of the membrane potential v_j of the jth neuron obey

$$C\frac{\mathrm{d}v_j}{\mathrm{d}t} = -g_{ca}m_{\mathrm{inf}}(v_j)(v_j - v_{ca}) - g_k w_j(v_j - v_k) - g_l(v_j - v_l) + I_j, \tag{1}$$

$$\frac{\mathrm{d}w_j}{\mathrm{d}t} = \phi\frac{[w_{\mathrm{inf}}(v_j) - w_j]}{\tau_w(v_j)}, \tag{2}$$

with

$$m_{\mathrm{inf}}(v) = 0.5[1 + \tanh\{(v - v_1)/v_2\}] \tag{3}$$

$$w_{\mathrm{inf}}(v) = 0.5[1 + \tanh\{(v - v_3)/v_4\}] \tag{4}$$

$$\tau_w(v) = 1/\cosh\{(v - v_3)/(2v_4)\}. \tag{5}$$

The parameters C, g_{ca}, g_k, g_l, v_{ca}, v_k, v_l, ϕ, v_1, v_2, v_3 and v_4 are adjusted in a way that the model fits the dynamical behavior of a population of STN neurons (Hauptmann and Tass 2007). The model parameters are given in the caption of figure 4.

The current I_j controls the dynamics of the spike generator and comprises several different currents:

$$I_j(t) = I_j^{\mathrm{slow}}(t) + I_j^{\mathrm{noise}}(t) + I_j^{\mathrm{const}} + X_{\mathrm{EXC}}s_1 I_j^{\mathrm{stim}}(t) + I_j^{\mathrm{syn}}(t) + I_j^{\mathrm{sen}}(t), \tag{6}$$

where $I_j^{\mathrm{stim}}(t)$ is the stimulation current, $I_j^{\mathrm{syn}}(t)$ is a current due to synaptic coupling and $I_j^{\mathrm{sen}}(t)$ is an additional sensory stimulation selectively driving neurons belonging to a particular sub-group of neurons. I_j^{slow} is a slowly varying current, which has been proposed as a burst generating mechanism by Rinzel and Ermentrout (1989). It is governed by

$$\frac{\mathrm{d}I_j^{\mathrm{slow}}}{\mathrm{d}t} = \varepsilon_j\left\{v^* - v_j(t - \tau_j) - \alpha I_j^{\mathrm{slow}} - X_{\mathrm{INH}}s_2\left|I_j^{\mathrm{stim}}(t)\right|\right\}, \tag{7}$$

where v^*, ε and α are parameters. The slowly varying current captures the inhibitory feedback from the GPe. This feedback pathway is subject to a time delay (Terman *et al* 2002; Hauptmann and Mackey 2003). Using I_j^{slow} provides a reasonable simplification of the model, see Hauptmann and Tass (2007, 2009).

$I_j^{\mathrm{noise}}(t)$ is a spatially incoherent exponentially correlated noise source of intensity D_{noise} and with a correlation time τ_{noise} that models noise introduced by external and internal

sources. The exponentially correlated noise was calculated using a second-order algorithm with a fixed step size (Dolan *et al* 1999) which is embedded into the variable step size Runge–Kutta method of fourth order used for the integration of the main time-delayed differential equation system (Hairer *et al* 1987). I_j^{const} is a constant current that adjusts the spike generator relative to the onset of the oscillatory behavior, which is required for the bursting activity. For more details on the dynamics of the model without the sensory input (i.e. for $I_j^{\text{sen}} = 0$ for all j), we refer to Hauptmann and Tass (2007, 2009).

2.1. Stimulation effects

Electrical stimulation of neuronal structures has both excitatory and inhibitory effects, which are mediated for example by activating the STN neurons or the axons passing from the GPe to the STN population, respectively (Benabid *et al* 2005). In our model, this is taken into account by the terms s_1 (equation (6)) and s_2 (equation (7)), which control the local effectiveness of the stimulation of excitatory (s_1) and inhibitory (s_2) structures, and the parameters X_{EXC} and X_{INH}, which control both the onset and offset of the stimulation and the amount of excitatory and inhibitory action of the stimulation ($X_{\text{EXC}} + X_{\text{INH}} = 1$ during stimulation, $X_{\text{EXC}} = X_{\text{INH}} = 0$ else). Since standard HF DBS produces similar clinical effects as lesions in various structures (Benabid *et al* 2005), it is assumed that the inhibitory effect of stimulation dominates the excitatory effect; therefore, the herein finally realized mechanism of the stimulation is a mixture of excitatory (30%) and inhibitory effects (70%) (Hauptmann and Tass 2007).

For the stimulation we use CR and HF stimulation acting locally in the neuronal network, i.e. the effectiveness of the stimulation decays with the distance from the electrode (Ranck 1975). The N STN neurons are randomly distributed in an elliptic shape schematically illustrating the STN structure, figure 1. A DBS electrode with four contacts (red colored) is placed within the target structure. The black dots indicate the positions of the neurons. Neurons receiving an additional sensory input $I_j^{\text{sen}}(t)$ are colored in blue (first microcircuit), yellow (second microcircuit) and red (third microcircuit). The stimulation effect decreases with increasing distance between the electrode and neuron following the function $K_{ij} = 1/(l d_{ij}\sqrt{1+4(d_{ij}/l)^2})$, where d_{ij} denotes the distance between the jth neuron and the center of the ith electrode (Richardson *et al* 2003) and $l = 1.5$ mm denotes the typical contact length of the Medtronic 3387 and 3389 DBS leads (Coffey 2009).

In our simulations, we use both high-frequency (HF) and coordinated-reset (CR) stimulation. Both stimulation patterns are composed of bi-phasic pulses, i.e. a short (0.2 ms) primary pulse is followed by a long (3 ms) secondary, charge-balancing pulse of opposite polarity. The pulses are either repeated continuously in a purely periodic manner (HF stimulation) or follow the CR stimulation pattern (figure 2). HF stimulation consists of a continuous pulse train composed of bi-phasic pulses repeated with a frequency of $F_{\text{HF}} = 130$ Hz. The stimulation is applied through the contact $C2$ (third contact from the tip, arbitrarily chosen without loss of generality) (figure 2(B)). In a large portion of patients treated with DBS, only one contact is activated for the application of HF stimulation (monopolar setting) (Rodriguez-Oroz *et al* 2005); therefore, this setting was exemplary chosen. The CR pattern consists of short pulse trains (composed of six bi-phasic pulses of width 0.2 ms for the primary pulse part and 3 ms for the secondary charge-balancing pulse part), which are sequentially applied at the four stimulation contacts. Each CR sequence (duration $\tau = 200$ ms, corresponding to a stimulation frequency of $F_{\text{CR}} = 5$ Hz) is followed by a pause of 200 ms duration (figure 2(C)).

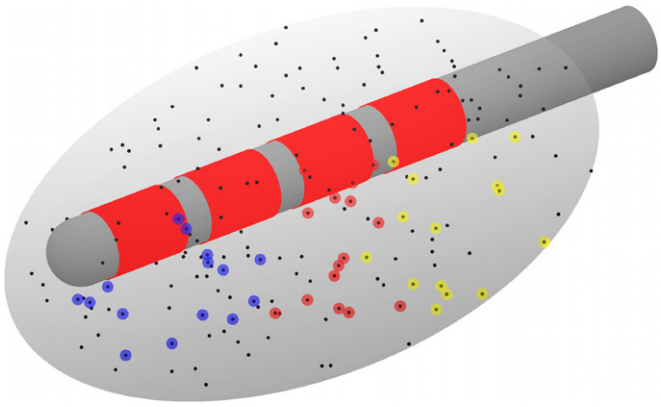

Figure 1. Schematic model of the used neuronal network. The $N = 200$ neurons are placed within the elliptic model STN. The DBS stimulation electrode is placed within the target structure; the metallic contacts are denoted by red color, separated by insulating parts (gray). The neurons of the three microcircuits receiving an additional sensory input are marked with blue (first microcircuit), yellow (second microcircuit) and red (third microcircuit) circles. Each microcircuit is formed by 15 neurons selected as the 15 nearest neighbors of the chosen center of the cluster.

2.2. Synaptic plasticity

Within the STN, neurons are coupled by excitatory synapses (Kita *et al* 1983; Shen *et al* 2003; Gillies and Willshaw 2004), where the synaptic interaction is modeled according to Terman *et al* (2002). All-to-all coupling is realized within the STN population, where the coupling strength is variable, following the plasticity rule introduced below. The post-synaptic effect of an action potential spreading from neuron j is calculated at the source neuron side. An action potential results in an opening of the ion gates associated with glutamatergic synapses present in the STN (Kita *et al* 1983; Shen *et al* 2003; Gillies and Willshaw 2004):

$$\frac{\mathrm{d}g_j^s}{\mathrm{d}t} = \alpha_s \frac{1}{1+\mathrm{e}^{-(v_j-\theta_s)/\sigma_s}}\left(1-g_j^s\right) - \beta_s g_j^s, \tag{8}$$

where α_s, θ_s, σ_s and β_s are parameters listed in the caption of figure 4. The resulting synaptic current $I_j^{\text{syn}}(t)$ driving the jth neuron is given by

$$I_j^{\text{syn}}(t) = -\bar{g}_s(v_j - v_s)\frac{1}{N}\sum_i s_{ij} g_i^s(t), \tag{9}$$

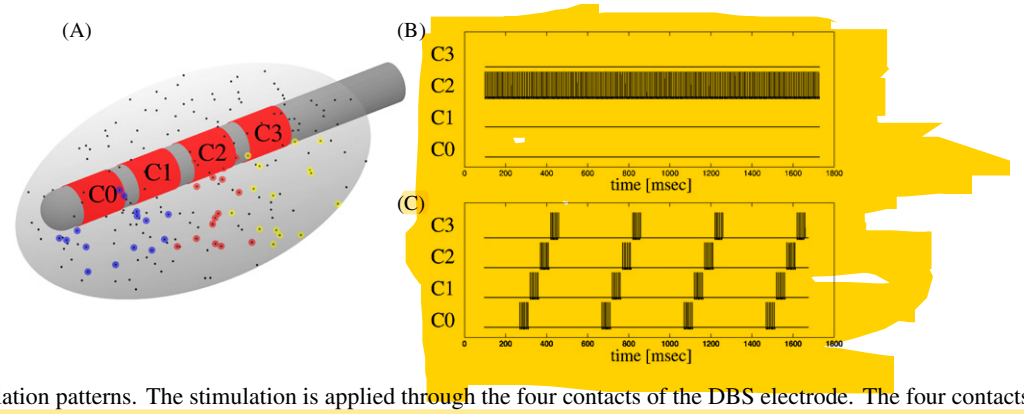

Figure 2. Applied stimulation patterns. The stimulation is applied through the four contacts of the DBS electrode. The four contacts are named $C0$–$C3$ (A). Through these contacts either a HF pattern is applied, where one contact is activated only (here, $C2$ (B)), or a CR pattern is applied, where the four contacts are activated sequentially (C). CR stimulation (C) consists of a repeated $CycOn = 1$, $CycOff = 1$ pattern.

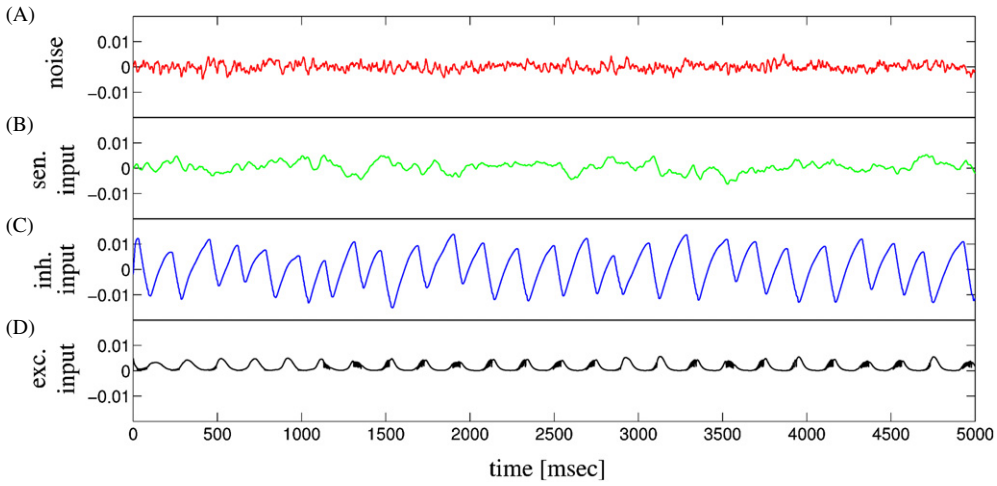

Figure 3. Comparison of the different neuronal inputs. The neurons are driven by spatially uncorrelated noise with weak amplitude (A). Selected neurons are additionally driven by the correlated input ($A_{\mathrm{sen}} = 0.0002$) with a longer decay time for the temporal correlation (B). The communication between the neurons is represented by the slowly varying input mediating the inhibitory connections from the GPe to the STN (C) and by the excitatory STN-STN input (D). The simulations show a network during synchronized activity.

where s_{ij} is the coupling coefficient from the ith and the jth neurons.

Experimental results demonstrate strong synaptic plasticity of the excitatory connections within the STN (Shen *et al* 2003), which is, hence, implemented in our model via the synaptic impact s_{ij} of each synapse, which can be changed within a specified interval following the learning rule introduced below.

In numerous experiments it has been demonstrated that the strength of the synaptical interaction changes depending on the relationship of the timing of pre- and post-synaptic neuronal activity (Gerstner *et al* 1996; Bi and Poo 1998; Bi 2002; Shen *et al* 2003). Bursting is the dominating pathological activity, experimentally observed in neuronal populations relevant for PD and other movement disorders (Beurrier *et al* 2002; Wichmann *et al* 1999). For this reason, our STN model neurons are bursters as well, and the activity-induced changes of the strength of the synapses are controlled by the timing of the bursts (Froemke and Dan 2002). A symmetric and smooth function controls the induced synaptic changes (Kepecs *et al* 2002; Wittenberg and Wang 2006; Pfister and Gerstner 2006): the change of the strength of the synapse from the ith to the jth neuron,

$$\Delta s_{ij} = c_P \, \mathrm{e}^{-|\mathrm{IBI}_{ij}|/\tau_P} - c_D \, \mathrm{e}^{-|\mathrm{IBI}_{ij}|/\tau_D}, \qquad (10)$$

depends on the inter-burst interval of these neurons, IBI_{ij}. The values of s_{ij} are restricted to the interval $[s_{\min}, s_{\max}]$. The synaptic strength increases if the two bursts are close to being coincident (<20 ms), whereas desynchronized bursting results in a decrease of the synaptic strength.

In other words, coinciding activity results in a potentiation of the synaptic connectivities while desynchronized activity results in a slow reduction of the synaptic connectivities within the range given by $[s_{\min}, s_{\max}]$.

2.3. Additional sensory input mimicking physiological afferent input

The target structure for DBS is part of a loop of nodes involved in the processing of e.g. movement-related information.

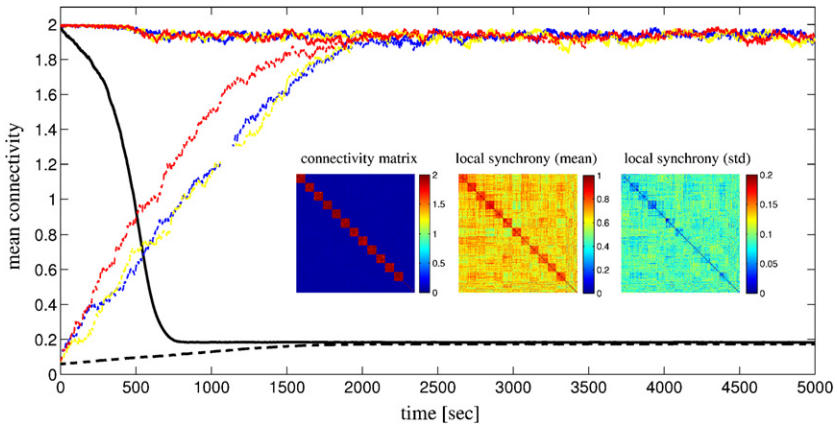

Figure 4. Normal sensory input-related activity (12 microcircuits with 15 neurons each) results in stable segregated microcircuits. The mean connectivity for the whole system (black curve) and for three exemplary microcircuits (blue, red and yellow curves). The connectivity matrix (left matrix) is evaluated during the last 10 s with the sensory input. Red (blue) values indicate high (low) connectivity. The enhanced local connectivity has a strong impact on the local synchrony (middle matrix) and the standard deviation of the local synchrony (right matrix). The system is initially starting from two different states, a state where all connectivities are high (solid curves) and a state where all connectivities are weak (dashed curves). The connectivity and synchrony matrices are displayed for the simulation initially started with high connectivities. Simulation parameters: $N = 200$, $A_{\text{sen}} = 0.0002$, $g_{ca} = 1.0$, $g_k = 2.0$, $g_l = 0.5$, $v_{ca} = 1.0$, $v_k = -0.7$, $v_l = -0.5$, $v_1 = -0.01$, $v_2 = 0.15$, $v_3 = 0.1$, $v_4 = 0.145$, $C = 1.0$, $\phi = 1.15$, $v^\star = -0.22$, $\alpha = 0.0$, $\tau_j = 10$, $\epsilon_j = 2 \times 10^{-3}(4 \times 10^{-6})$ Gaussian distributed with mean (standard deviation), $\alpha_s = 0.1$, $\beta_s = 0.05$, $\theta_s = 0.2$, $\sigma_s = 0.02$, $\bar{g}_s = 1.0$, $v_s = 0.3$, $D_{\text{noise}} = 0.00002$, $\tau_{\text{noise}} = 5$, $I_j^{\text{const}} = 0.075$, $c_P = 0.038$, $\tau_P = 10$, $c_D = 0.02$, $\tau_D = 25$, $s_{\min} = 0.05$, $s_{\max} = 2$.

Different segregated portions of the STN are responsible for the processing of different sensory information (Bergman *et al* 1998; Pessiglione *et al* 2005) . To represent this process in our simplified model system, we added the sensory input $I_j^{\text{sen}}(t)$ to selected neurons (figure 1). A small number of microcircuits is selected (e.g. three in figure 1) and each microcircuit contains M neurons, which are nearest neighbors to the chosen center of the cluster (e.g. $M = 15$ in figure 1). The microcircuit topology is motivated by a tracing study aiming at the elucidation of the organization of the interconnections between the subthalamic nucleus and the two segments of the globus pallidus in squirrel monkeys (Shink *et al* 1996). Together with the limitations given by the comparable small number of neurons in our model network, we maximally consider 12 segregated microcircuits. Each microcircuit is assumed to cover 5–10% of the STN, which might be in qualitative agreement with figures 4 and 5 in Shink *et al* (1996), while the simultaneous staining of neighboring fibers (or even microcircuits) in the tracer study might be the cause of the observed relatively large size of the individual microcircuits. Finally, the number of neurons within each cluster is given by the total number of neurons within the STN network divided by the estimated number of functional microcircuits (in our simulation we considered up to 12 clusters containing 15–30 neurons each). Each neuron from one microcircuit receives the same sensory input. The input is formed by an exponentially correlated stochastic source of intensity A_{sen}. The correlation time τ_{sen} for the sensory input is chosen to be large (in our simulations we use $\tau_{\text{sen}} = 25$ ms). The stochastic sensory input A_{sen} is calculated using a second-order algorithm with a fixed step size (Dolan *et al* 1999). The additionally noisy input $I_j^{\text{noise}}(t)$, which is different for each neuron, guarantees that no neuron receives exactly the same input as another neuron.

The sensory input $I_j^{\text{sen}}(t)$ (B, the green line in figure 3) is of the same order of magnitude as the noise term $I_j^{\text{noise}}(t)$ (A, the red line in figure 3) and the synaptic communication within the STN $I_j^{\text{syn}}(t)$ (D, the black line in figure 3). Note that data are obtained from a system in the synchronized mode, where the synaptic communication is highly correlated, which results in an oscillatory synaptic input. In contrast, in the desynchronized case, the amplitude of the variations of $I_j^{\text{syn}}(t)$ is much smaller. The recurrent inhibition from the GPe I_j^{slow} is much stronger than the other three contributions (C, the blue line in figure 3). In our model setup, each STN neuron is connected with one GPe neuron; hence, the strong inhibition mediated by the GPe neurons, which is responsible for the generation of the bursting activity, is similar for the synchronized and desynchronized modes.

To analyze the extent of segregation of the microcircuits with respect to the rest of the neuronal network, we utilize the local synchronization of the neurons of the network. The idea behind this approach is that neurons that fire together wire together and vice versa (Hebb 1949). Accordingly, the local synchronization indicates to what extent two neurons out of the network show correlated activity. The local synchrony is evaluated with the synchronization index

$$\tilde{R}_{ij}(t) = \tfrac{1}{2}|\exp[-\mathrm{i}2\pi(\phi_i(t) - \phi_j(t))]|, \qquad (11)$$

where $\phi_i(t)$ and $\phi_j(t)$ are the phases of neurons i and j at time t, respectively (Pinsky and Rinzel 1995). The synchronization index $R_{ij}(t)$, which is bounded to the interval $[0, 1]$, is averaged within non-overlapping time windows of 10 s duration: $R_{ij}(t) = \langle \tilde{R}_{ij}(t) \rangle_{10\,\text{s}}$, where $\langle \cdots \rangle_{10\,\text{s}}$ denotes an averaging around t in a 10 s window.

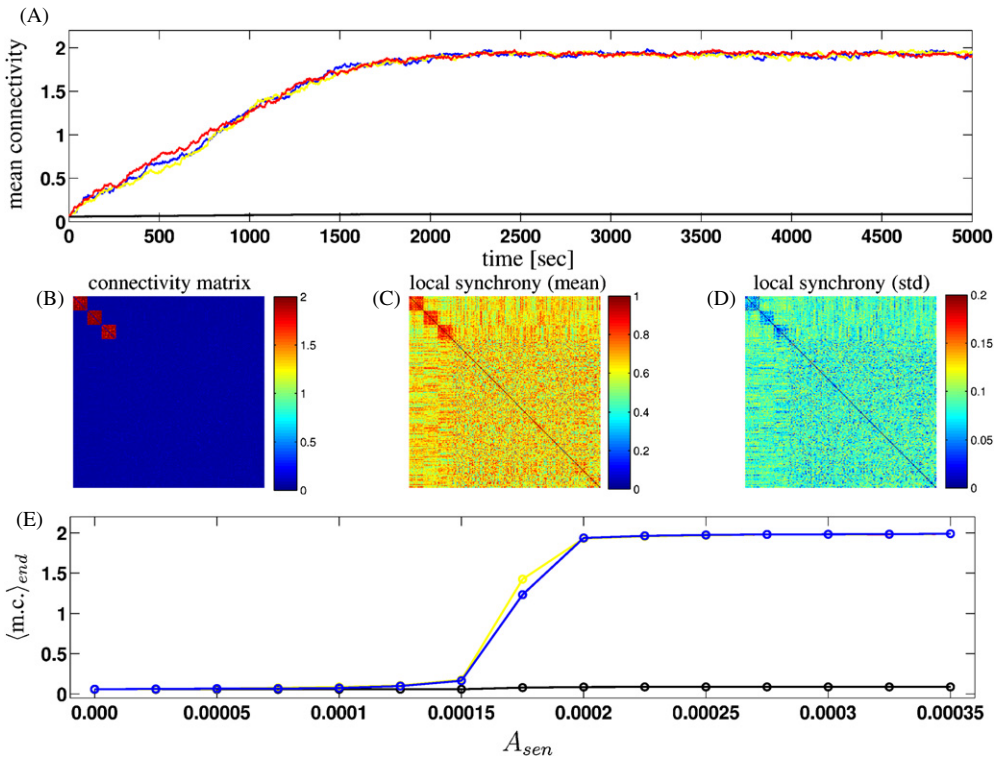

Figure 5. Effect of a segregated sensory input into three microcircuits, formed by 15 neurons each, on the connectivity of the network. No therapeutic stimulation is delivered ($I_j^{\text{stim}} = 0$ for all j). (A) The mean connectivity for the whole system (black line) and for the three microcircuits (blue, red and yellow lines). (B) The connectivity matrix is evaluated during the last 10 s with the sensory input. Red (blue) values indicate high (low) connectivity. The enhanced local connectivity (B) has a strong impact on the local synchrony (C) and the standard deviation of the local synchrony (D). (E) Dependance of the final connectivity pattern on the amplitude of the sensory input A_{sen}. $\langle m.c.\rangle_{\text{end}}$ stands for the mean connectivity (i.e. mean synaptic weight averaged within the final 10 s window). The system is initially starting from a state where all connectivities are weak. The same colors are used as in subplot (A). Note that the red curve is covered by the blue curve. Simulation parameters: $A_{\text{sen}} = 0.0002$ (A)–(D), and other parameters as in figure 4.

Based on this local synchronization index, we can calculate the extent of segregation of the neurons within the functional microcircuit k as

$$S_k^{\text{syn}}(t) = \frac{1}{M^2} \sum_{i,j \in \text{microcircuit } k} \langle R_{ij}(t)\rangle_{10\,\text{s}} - \frac{1}{M\cdot(N-M)} \sum_{i \in \text{microcircuit } k,\, j \notin \text{microcircuit } k} \langle R_{ij}(t)\rangle_{10\,\text{s}}. \tag{12}$$

$S_k^{\text{syn}}(t) = 1$ denotes a maximal segregation, i.e. the activity of the microcircuit k is isolated from (i.e. uncorrelated with) the activity of the rest of the network and the neurons from within the microcircuit k show synchronized activity. In contrast, $S_k^{\text{syn}}(t) = 0$ denotes the case where the neurons of the microcircuit show no segregated activity. A loss of segregation can result in different behavior, either the neurons within the microcircuit k are uncorrelated with each other and with the rest of the network or all neurons of the network are in synchrony with each other.

A second measure of the extent of connection-wise segregation of the neurons within the functional microcircuit k is based on the connectivities within the microcircuits and from each microcircuit to the rest of the population:

$$S_k^{\text{con}}(t) = \frac{1}{M^2} \sum_{i,j \in \text{microcircuit } k} \langle s_{ij}(t)\rangle_{10\,\text{s}} - \frac{1}{M\cdot(N-M)} \sum_{i \in \text{microcircuit } k,\, j \notin \text{microcircuit } k} \langle s_{ij}(t)\rangle_{10\,\text{s}}. \tag{13}$$

$S_k^{\text{con}}(t) = s_{\max}$ denotes a maximal segregation, i.e. the microcircuit k is isolated from the rest of the network. In contrast, $S_k^{\text{con}}(t)$ close to zero denotes the case where the connectivities within the microcircuit and from the microcircuit to the rest of the population are similar.

All system parameters are adjusted such that a bursting activity and an interaction between the STN neurons emerges that is comparable to neuronal activity observed in experimental studies (Bergman *et al* 1994; Nini *et al* 1995; Smirnov *et al* 2008). In these experimental studies, rhythmic activity of single neurons (Bergman *et al* 1994; Nini *et al* 1995) and oscillatory activity of the local field potential (Smirnov *et al* 2008) close to the tremor frequency were observed. The basic parameters of the Morris–Lecar equation (1)–(5) and of the slowly varying current (7) were taken from a theoretical study investigating the dynamical property of the generic burst generator (Rinzel and Ermentrout 1989). The

bursts, generated by the modified Morris–Lecar system, show the characteristics (e.g. frequency and pattern) of the bursts observed in experimental studies (Bergman *et al* 1994; Nini *et al* 1995). The parameters controlling the application of the stimulation pulses are chosen such that the stimulation reaches most of the neurons within the network. The parameters of the synaptic transmission are adjusted corresponding to the dynamical properties of the glutamatergic synapses of the STN neurons (Shen and Johnson 2006). A fast onset time of the excitatory postsynaptic potential (EPSP), corresponding to a small value of α_s, is accompanied by a slower decay rate of the EPSP after burst offset, corresponding to a larger value of β_s. The latter results in decay rates of approximately 20 ms as observed in experimental studies (Shen and Johnson 2006).

In what follows we will investigate to what extent this weak sensory input, mimicking the processing of the segregated afferent input, is able to generate segregated microcircuits of inter-connected neurons.

3. Results

3.1. Normal physiological sensory input

First, we study the behavior of the STN under normal sensory input-related activity. From Shink *et al* (1996) we estimated the number of distinct microcircuits in a neuronal area as small as the STN. Since approximately 5–10% of the STN is covered by a single microcircuit, we use a total number of 12 microcircuits. Each microcircuit is formed by 15 neurons situated near each other. Each neuron from one microcircuit receives the same sensory input. We perform a simulation to evaluate if such a normal sensory input-related activity results in a stable state of the network formed by segregated microcircuits with no pathological activity. Therefore, the STN is initialized in two different states, a state where all connectivities are weak and a state where all connectivities are high (figure 4). Both simulations finally approach the same state, where the connectivity only within each microcircuit shows a high level but the microcircuits are segregated. Note that for illustration purposes the mean connectivity within the first three microcircuits is shown (figure 4, blue, red and yellow curves). The overall mean connectivity approaches a low level independent of the initial state (figure 4, black curves). The finally approached level of approximately 0.18 reflects the high connectivity levels (close to $s_{\max} = 2.0$) within the microcircuits and the low level of connectivity between neurons not belonging to the same microcircuit (close to $s_{\min} = 0.05$). The topology of the connectivity pattern is visualized in the connectivity matrix, where the neurons are arranged with respect to their microcircuit allocation (figure 4, left matrix). The local synchrony (figure 4, middle matrix) and the corresponding standard deviation (figure 4, right matrix) support the hypothesis that due to the sensory input-related activity, the microcircuits establish segregated activity. Local synchrony can be found within each microcircuit, while the correlation with the neurons outside the particular microcircuit shows a low level of synchrony with higher fluctuations (figure 4, middle and right matrices). The mean local synchrony level within the microcircuits is $\langle R_{ij}(t)\rangle = 0.81$ (the average over all neuron-to-neuron connectivities within the 12 microcircuits was taken), while the synchrony with other neurons within the network is considerably lower ($\langle R_{ij}(t)\rangle = 0.65$). The segregation level based on the local synchrony therefore denotes $\langle S^{\text{syn}}\rangle = 0.16$ (equation (12), again the average is taken over all 12 microcircuits). The segregation level based on the connectivities denotes $\langle S^{\text{con}}\rangle = 1.86$ (equation (13), again the average is taken over all 12 microcircuits evaluated at $t = 5000$ s). Note that the given values are taken from the simulation with initially high connectivities. The corresponding values of the simulation with initially low connectivities are very close to the given values (within 3%); therefore, the finally realized states are considered to be similar.

Recent results indicate that the genesis of the pathophysiology of Parkinsonian disease is associated with a sensory deficit which results in a deafferentation of the sensory input (Nolano *et al* 2008). This peripheral deafferentation was causally related to the impairment of sensory function in Parkinson's disease (Nolano *et al* 2008). Deafferentation is observed in other diseases and was identified as the one reason for the emergence of pathological, in particular phantom phenomenon-like rhythmic activity (Weisz *et al* 2007; De Ridder *et al* 2007; Bonilha *et al* 2010). Therefore, we consider a situation with a reduced number of microcircuits driven by sensory input-related activity as a potential candidate for a Parkinsonian state. In the following we will investigate to what extent such a reduced sensory input is capable of inducing multistability and of provoking the development of synchronized pathological activity in the STN.

3.2. Reduced sensory input

Starting from a network with low average connectivity, the application of the sensory input to only three distinct sub-populations of the network (formed by 15 neurons each) results in the generation of three microcircuits. The latter are characterized by a high connectivity within the microcircuit while the neurons of a microcircuit show only weak connectivity to the neurons not belonging to that particular microcircuit (figure 5).

Because of the weak sensory input to the three distinct sub-populations ($A_{\text{sen}} = 0.0002$) and because of the slow time scale of the changes of the connectivity mediated by synaptic plasticity, the microcircuits need 2000 s to be completely established (figure 5(A)). The mean connectivity within the three microcircuits (represented by the red, blue and yellow lines) reaches a value close to the maximal connectivity value of $s_{\max} = 2$ and stays there after a transient period of 2000 s. The mean connectivity (A, black line), calculated from all connectivities, is only slightly increased because the three microcircuits contain only 22.5% of the total number of neurons. This increase from initially 0.058 to 0.087 results from the contribution of the connectivities within the three microcircuits to the overall mean connectivity. The connectivity matrix evaluated at the end of the simulation (i.e. the averaged values of the last 10 s of the simulation)

shows the three strongly interconnected microcircuits (figure 5(B), red), while the connectivity of all other neurons is weak (blue). The sensory input promotes synchronized activity, and the enhanced connectivity within the microcircuit furthermore stabilizes the synchronized activity.

At the end of the simulation the neurons from within the three microcircuits are synchronized, while the local synchronization (equation (11)) between neurons not belonging to the same microcircuit is comparably weak (figure 5(C)). The standard deviation of the local synchronization in the evaluation interval is slightly smaller within the microcircuits (figure 5(D)). At the end of the simulation the three microcircuits are segregated with respect to their mutual synchronization. The mean values of the local synchrony within the microcircuits (equation (11)) lie within the interval $\langle R_{ij}(t)\rangle \in [0.82, 0.84]$ (the brackets $\langle\rangle$ indicate averaging for all i, j belonging to a microcircuit), while the mean synchrony between a neuron of a certain microcircuit and a neuron not belonging to that microcircuit lies within the interval $\langle R_{ij}(t)\rangle \in [0.63, 0.64]$. Hence, the values indicating the segregation of the microcircuits is $S_1^{\mathrm{syn}} = 0.21$, $S_2^{\mathrm{syn}} = 0.20$, $S_3^{\mathrm{syn}} = 0.19$ (equation (12)) and $S_1^{\mathrm{con}} = 1.87$, $S_2^{\mathrm{con}} = 1.89$, $S_3^{\mathrm{con}} = 1.85$ (equation (13)), where indexes 1, 2 or 3 refers to the three microcircuits driven by the sensory input.

The generation of the interconnected microcircuits strongly depends on the amplitude of the sensory input A_{sen}. Only if the sensory input is strong enough, i.e. $A_{\mathrm{sen}} > 0.000\,175$, do distinct microcircuits emerge (figure 5(E)). For amplitudes below that critical value, the sensory input is not able to establish clustered connectivities. Even small sub-populations (containing, say, five neurons) driven by a sufficiently high sensory input can result in the emergence of a clustered connectivity structure in the network (data not shown). To test this, we varied the number M of neurons in each of the three microcircuits from 5 to 30. Even the driving of five neurons with a common sensory input is able to generate an inter-connected microcircuit if the network initially starts with low connectivities.

3.3. Effects of the sensory input on the stability of pathological synchrony

Starting from a network with strong neuronal connectivities, which result in a mostly synchronized and pathological activity, the effects of the sensory input are investigated. Depending on the strength and pattern of the sensory input, finally different activity patterns emerge, which can be characterized by their level of segregation of the microcircuit activity linked to the sensory input and by the level of residual synchronized, pathological activity.

Let us consider four different scenarios, which differ with respect to the number of neurons driven by the sensory input and the strength of the sensory input (figure 6). The weak sensory input (in figure 6 the same amplitude $A_{\mathrm{sen}} = 0.0002$ is used as in figure 5) is neither capable of resolving the synchronized activity nor of restoring the segregation of the microcircuited activity (figures 6(A) and (B)). The mean connectivity is only slightly decreased in the course of the stimulation (figure 6(A), black line). The matrix representation of the connectivity (figure 6(A) inset) shows that the three microcircuits are no longer connected to each other, but the neurons of the microcircuits are still strongly connected to the many neurons outside the microcircuits. In other words, due to the weak sensory input, the direct interaction between the microcircuits vanishes. However, they are still indirectly interacting via the neurons outside the microcircuits. Consequently, there is a strong overall synchronization and in particular also a strong synchronization between the different microcircuits (figures 6(A) inset and (B)). Accordingly, the level of segregation (equations (12) and (13)) is close to zero ($S_k^{\mathrm{syn}} \in [0.03, 0.05]$, $S_k^{\mathrm{con}} \in [0.34, 0.36]$). Hence, the weak sensory input is not able to establish a segregation of the functional microcircuits if the network is initialized in the synchronized state.

In contrast, stronger stimulation (figure 6(A), blue line $A_{\mathrm{sen}} = 0.0004$) decouples the distinct microcircuits both from each other and from the neurons outside the microcircuits. Hence, the sufficiently strong sensory input wipes out both direct and indirect interactions between the microcircuits. Consequently, synchronization emerges only within the microcircuits and among the neurons outside the microcircuits (figures 6(A), inset and (C)). The segregation value for the three microcircuits lies within $S_k^{\mathrm{syn}} \in [0.13, 0.33]$ $\left(S_k^{\mathrm{con}} \in [1.93, 1.94]\right)$. Nevertheless, being restricted to only a smaller part of the population, the comparably strong sensory input is not able to abolish the synchronization among the neurons outside the microcircuits.

If the portion of the neurons that receive the sensory input is increased from $M = 15$ to $M = 30$ per microcircuit, the already weak sensory input ($A_{\mathrm{sen}} = 0.0002$) is sufficient to induce a segregation of the three microcircuits $\left(S_k^{\mathrm{syn}} \in [0.21, 0.31], S_k^{\mathrm{con}} \in [1.90, 1.91]\right)$ (figures 6(A) and (D)). Moreover, with six (instead of three) microcircuits, each consisting of 30 neurons (figures 6(A) and (E)), not only is a segregation of the microcircuits achieved $\left(S_k^{\mathrm{syn}} \in [0.12, 0.27], S_k^{\mathrm{con}} \in [1.90, 1.91]\right)$, but also an extinction of the synchronization in the small residual sub-population.

To conclude, the weak sensory input driving a small portion of the whole network is not able to establish a segregated microcircuit activity. Only if the sensory input covers a larger portion of the population with pathological activity, are both the extinction of synchronized activity and the segregation of the microcircuits achieved.

3.4. Effects of DBS on the microcircuit segregation

Electrical HF DBS is a well-established treatment for patients suffering from medically refractory Parkinson's disease (Benabid *et al* 2009). HF DBS is an acute therapy used to reduce Parkinsonian symptoms. These acute effects of HF DBS vanish immediately after stimulation offset so that the Parkinsonian symptoms (Temperli *et al* 2003) and the symptom-related β-activity (Kühn *et al* 2008) revert back immediately. In contrast, CR DBS aims at inducing a long-lasting desynchronization achieved by rewiring the

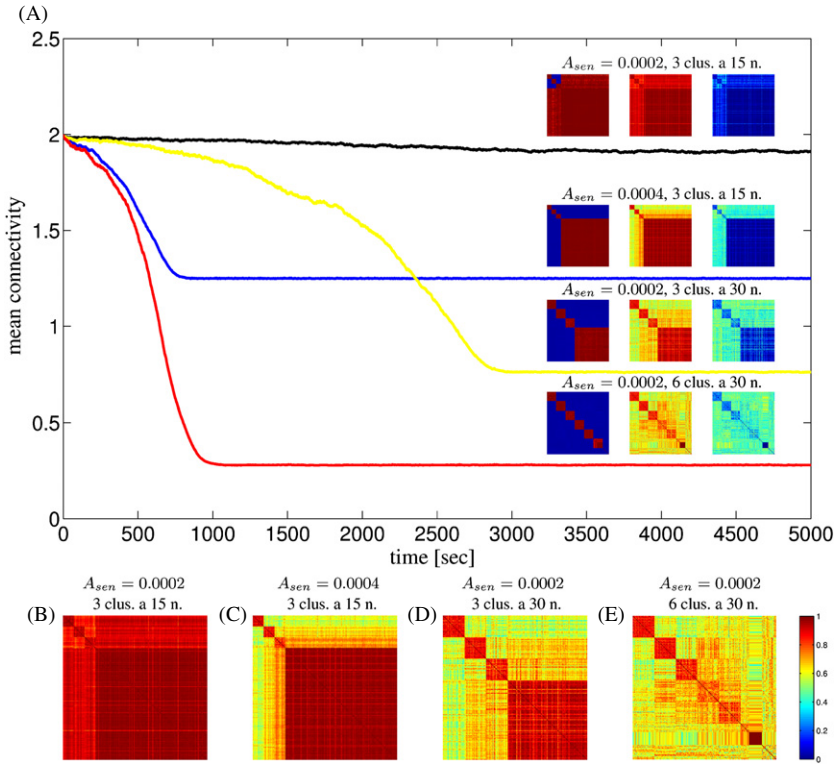

Figure 6. Effect of the sensory input on synchronized activity as observed during the pathological condition. The network is initialized with high connectivities on all possible synaptic connections. Four different parameters and setups for the sensory input are evaluated and plotted. (i) The weak sensory input ($A_{\text{sen}} = 0.0002$, 3 microcircuits with 15 neurons each) results in a mild reduction of the mean connectivity (A, black line). (ii) The strong sensory input ($A_{\text{sen}} = 0.0004$, 3 microcircuits with 15 neurons each) results in a stronger reduction of the mean plasticity (A, blue line) and generates segregated microcircuits. (iii) Larger microcircuits driven by the weak input ($A_{\text{sen}} = 0.0002$, 3 microcircuits with 30 neurons each) also result in a reduction of the mean plasticity (A, yellow line), while (iv) a higher number of microcircuits including a larger number of neurons ($A_{\text{sen}} = 0.0002$, 6 microcircuits with 30 neurons each) results in the most prominent reduction of the mean connectivity and abolishes the synchrony in the pathological sub-population (A, red line). The mean connectivity within the driven microcircuits stays high for the whole simulation period (not plotted). The matrices of the mean connectivity, of the mean local synchrony, of mean local standard deviation and of the synchrony evaluated during the last 10 s (from left to right), are plotted above the corresponding curves in (A). Enlarged plots for the mean local synchrony for the weak sensory input (B), strong sensory input (C), larger size of the microcircuits (D) and higher number of larger microcircuits (E).

stimulated network. Since experimental findings show that a loss of the functional segregation might be relevant to the pathophysiology of PD, we investigate how the segregation (represented in a simplified form in our model system through the segregation of microciruits) is affected by different forms of deep brain stimulation.

For HF and CR DBS, we show the time course of the mean connectivity within the whole population (black curve) and within the three microcircuits (blue, yellow and red curves) in figure 7(A). We apply HF and CR stimulations in the time interval from 200 to 3000 s (indicated by the red solid bar). The mean connectivity (m.c.) in the whole population (figure 7(A), black curve) rapidly decreases in the presence of CR stimulation (left, stimulation amplitude $A_{\text{stim}} = 1.2$). The mean connectivities within the three microcircuits, which are continuously driven by the sensory input, stay on a comparably high level ($\text{m.c.}_k(t) \in [1.12, 2]$). After the offset of the stimulation at $t = 3000$ s, the mean connectivities in the three microcircuits approach the maximally possible connectivity level $s_{\max} = 2$, and the m.c. approaches a level close to zero. Put otherwise, only sensory input-related connectivity outlasts CR stimulation.

In contrast, HF DBS of the same amplitude ($A_{\text{stim}} = 1.2$) results only in a moderate reduction of the mean connectivity during stimulation (figure 7(A), right, black curve). The mean connectivities within the three microcircuits stay on high levels (except for one microcircuit, blue curve). After stimulation offset only the microcircuit denoted by the blue curve reaches higher values of the mean connectivity, while the other values of the mean connectivity within the microcircuit are stabilized at considerably lower values (figure 7(A), right, blue, red and yellow curves). The overall mean connectivity is only slightly reduced by HF DBS. Note that the connectivity within two of the microcircuits (yellow and red curves) falls below the overall mean connectivity (figure 7(B), right). In other words, after HF stimulation offset, the pathologically upregulated overall connectivity outlives only slightly diminished, in some sense even at the expense of the sensory input-related connectivity.

For CR DBS the calculated time-dependent segregation $S_k^{\text{con}}(t)$ and $S_k^{\text{syn}}(t)$ shows that during stimulation the functional segregation already reaches a considerably high level of $S_k^{\text{con}}(t) \in [0.04, 1.46]$ (figure 7(B)) and $S_k^{\text{syn}}(t) \in [0.05, 0.178]$ (figure 7(C)). Without stimulation $S_k^{\text{con}}(t) =$

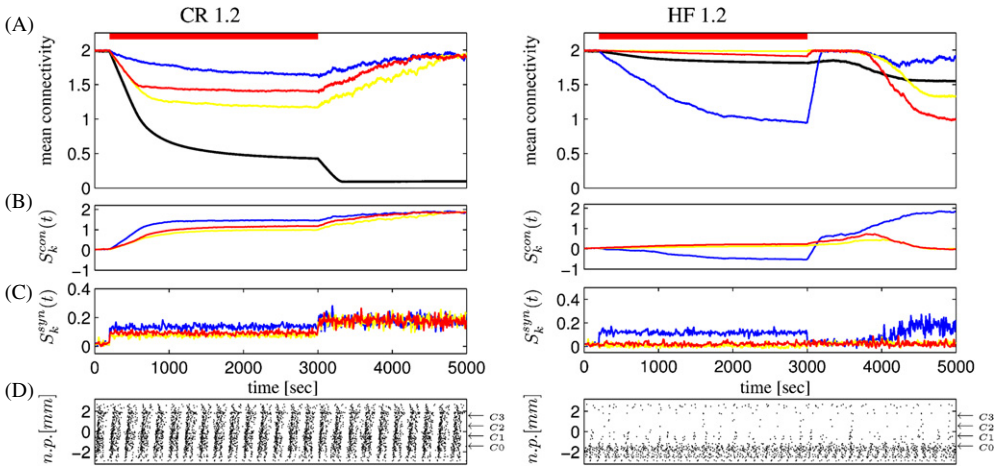

Figure 7. Effect of DBS on the sensory input-related microcircuits. The network is initialized with high connectivities on all possible synaptic connections. Coordinated reset (CR, left) and high-frequency (HF, right) stimulation are applied to the system. The sensory input is identical for all plots ($A_{\text{sen}} = 0.0002$, 3 microcircuits with 15 neurons each). The evolution of the mean connectivity and connectivity within the microcircuits (A) in the presence of CR and HF stimulation (stimulation amplitude $A_{\text{stim}} = 1.2$) and segregation values $S_k^{\text{con}}(t)$ (B) and $S_k^{\text{syn}}(t)$ (C) are plotted. The bursting activity during stimulation is illustrated by plotting a 5 s window (D), each dot indicates the onset of a burst. On the y-scale, the dots are arranged with respect to their projection to the stimulation lead; the position of the four lead contacts $C0$ to $C3$ is indicated on the left side of each plot. Stimulation parameters: $F_{\text{CR}} = 5$ Hz ($\tau = 200$ ms), $s_{\text{EXC}} = 1$, $s_{\text{INH}} = 10$, $C_{\text{inh}} = 70\%$ ($X_{\text{EXC}}(t) = 0.3$ and $X_{\text{INH}}(t) = 0.7$) for $t \in [200, 3000]$, $X_{\text{EXC}}(t) = 0$ and $X_{\text{INH}}(t) = 0$ else, $t_{\text{end}} = 3000$ s, $A_{\text{stim}} = 1.2$, $\tau_1 = 0$, $\tau_2 = \tau/4$, $\tau_3 = \tau/2$ and $\tau_4 = 3\tau/4$, $F_{\text{HF}} = 130$ Hz.

0.031 ($S_k^{\text{syn}}(t) = 0.019$) at the beginning of the simulation. The segregation values for the three microcircuits are shown as blue $\left(S_1^{\text{con/syn}}(t)\right)$, yellow $\left(S_2^{\text{con/syn}}(t)\right)$ and red $\left(S_3^{\text{con/syn}}(t)\right)$ curves (figures 7(B) and (C)). The segregation values are calculated from the connectivity pattern (equation (13), figure 7(B)) and from the local synchrony (equation (12), figure 7(C)) within the network. After stimulation offset both $S_k^{\text{con}}(t)$ and $S_k^{\text{syn}}(t)$ further increase and reach levels similar to the levels reached at the end of the simulation of figure 5. Five seconds of bursting activity (figure 7(D)) show that under CR stimulation the neurons continue to burst (left), whereas HF stimulation nearly completely suppresses the neuronal activity. The bursting activity is presented as a function of time (x-scale) and with respect to its projection along the stimulation electrode (y-scale). Each dot represents the onset of a burst. The contacts of the electrode are at the positions ($C0$: -1.45 mm, $C1$: -0.45 mm, $C2$: 0.55 mm, $C3$: 1.55 mm) in the coordinates of the y-scale shown in figure 7(D). Contact $C2$ is used for the application of HF stimulation, which is reflected by a local suppression of neuronal activity around the position of contact $C2$ in figure 7(D), right. In contrast, due to the pauses after each sequence of CR stimulation, the neuronal activity is not suppressed even in the case of strong CR stimulation (figure 7(D) left). Note that to achieve an STDP-mediated anti-kindling most efficiently, it is crucial that the neuronal activity is not suppressed.

For five values of the stimulation amplitude (A_{stim} increasing from 1.2 to 2.8 in steps of 0.4), the local synchrony pattern is displayed in figure 8 for CR (A) and HF (B) stimulation. The local synchrony pattern is calculated at the end of the simulation ($t = 5000$ s). For CR stimulation only the local synchrony not belonging to the functional microcircuits is reduced, while the synchrony within the microcircuits stays on the desired high level (indicated by the small red squares in figure 8(A)). Segregated neuronal activity is realized for all values of A_{stim}. In contrast, HF stimulation does not enable a segregation of the neuronal activity (figure 8(B)). Only for weak HF stimulation ($A_{\text{stim}} = 1.2$), can partly segregated microcircuits be observed. For higher values of $A_{\text{stim}} \geqslant 1.6$, HF stimulation has nearly no long-lasting effect on the connectivity pattern (figure 8(B)).

The simulation outcome is summarized in figures 8(C)–(F). Four measures are used for evaluation: first, the mean segregation level (equation (12)) is averaged over the whole stimulation epoch (figure 8(C)); second, the effect on the mean connectivity is analyzed by calculating the time $t_{\langle p\rangle_N < 0.1}$ needed until the mean connectivity falls below the level 0.1 (figure 8(D)); third, the total amount of stimulation applied to the network is calculated by a multiplication of the pulse rate (SR) with the stimulation amplitude (A) (figure 8(E)) and, fourth, the mean connectivity is evaluated at the end of the simulation (F). The averaged segregation during stimulation $\left\langle S_k^{\text{syn}}(t)\right\rangle_{\text{stim}}$ is high and independent of the stimulation amplitude for CR stimulation (figure 8(C)). HF stimulation only results in a slight increase in the level of segregation $\left\langle S_k^{\text{syn}}(t)\right\rangle_{\text{stim}}$ during the stimulation period (figure 8(C)). The red (gray) line indicates the mean value ($\pm$ standard deviation) in the stimulation-free case. The finally realized segregation $S_k^{\text{con}}(t)$ ($S_k^{\text{con}}(t) = 1.86$ for CR stimulation and $S_k^{\text{con}}(t) = 0.34$ for HF stimulation, mean values at the end of the simulation) shows similar behavior, while during stimulation strong CR stimulation does not result in an increase of $\left\langle S_k^{\text{con}}(t)\right\rangle_{\text{stim}}$; all connectivities are reduced by strong CR stimulation. For strong CR stimulation after stimulation, the segregated connectivity pattern is established. With HF stimulation no anti-kindling is achieved. Accordingly, the mean connectivity never reaches the threshold of 0.1

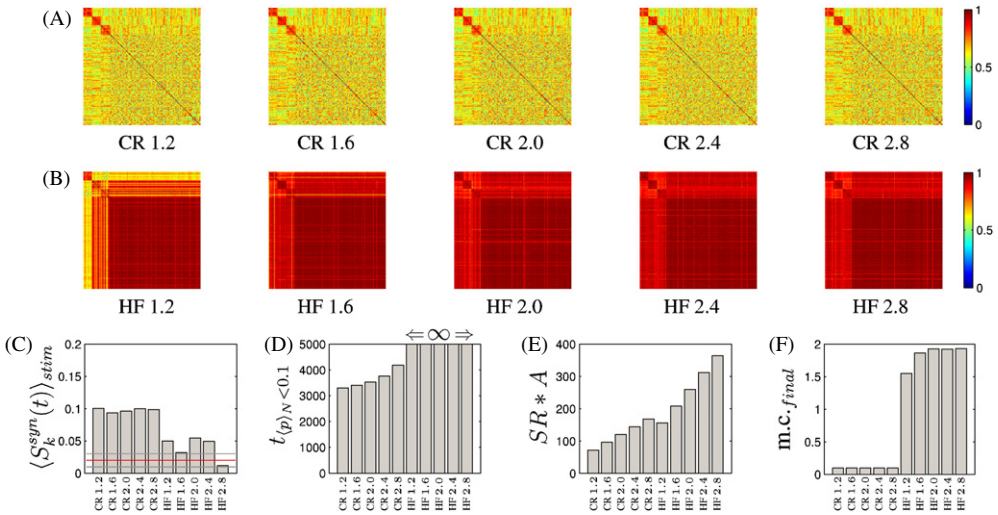

Figure 8. Effect of coordinated reset (CR) and high-frequency (HF) DBS of different amplitude on the sensory input-related microciruits. The network is initialized at a high level of all possible synaptic connections. Either CR or HF stimulation is applied to the system. The sensory input-related activity is identical for all plots ($A_{\text{sen}} = 0.0002$, 3 microcircuits with 15 neurons each). The mean local synchrony at $t = 5000$ s is plotted for CR (A) and HF (B) stimulation for different stimulation amplitudes increasing from 1.2 to 2.8 in steps of 0.4 (from left to right). In (C) to (F), the effect of CR and HF stimulation of different amplitude ($A_{\text{stim}} = 1.2$ to 2.8) is evaluated by calculating the mean segregation value during stimulation $S_k^{\text{syn}}(t)_{\text{stim}}$ (C, the mean value ($\pm$ standard deviation) for the stimulation-free case is indicated by the red (gray) line), the time it takes to achieve an anti-kindling, i.e. the time $t_{\langle p\rangle_N<0.1}$ until the mean plasticity (black curve in (A)) falls below 0.1 (D, the ∞ symbol above the HF results indicates that for HF stimulation the mean plasticity is stabilized on a high value), a measure representing the stimulation strength (stimulation rate SR times stimulation amplitude A) (E) and the mean connectivity $m.c._{\text{final}}$ at the end of the simulation (F). Stimulation parameters: $C_{\text{inh}} = 70\%$ ($X_{\text{EXC}}(t) = 0.3$ and $X_{\text{INH}}(t) = 0.7$) for $t \in [10, 3000]$, and other parameters as in figure 7.

(figure 8(D), indicated by the ∞ symbol), and the final level of the mean connectivity at the end of the simulation (figure 8(F)) indicates that HF stimulation is not capable of reducing the pathological connectivities. In contrast, CR stimulation results in the fast reduction of the pathological connectivities, which is reflected by the short time the mean connectivity needs to cross the level of 0.1 $t_{\langle p\rangle_N<0.1}$ (figure 8(D)). Please note that in all simulations the threshold of 0.1 is crossed shortly after stimulation offset (at $t = 3000$ s). For all values of A_{stim}, CR stimulation finally results in the complete reduction of the pathological connectivities (figure 8(F)). Moreover, to achieve this, CR stimulation requires considerably less energy compared to HF stimulation (figure 8(E)). CR stimulation applied with the parameters used in these simulations needs approx. 54% less stimulation if compared to HF stimulation of the same amplitude.

The segregation of the sensory input-related microcircuits is highest for weak and medium CR stimulation (figure 8(C)). HF stimulation fails to induce a restoration of segregated microcircuits during stimulation, i.e. the mean segregation value during stimulation does not exceed the value of 0.055 (figure 8(C)). Due to the strong and permanent stimulation, the neuronal activity during stimulation is blocked in the vicinity of the activated contact (figure 7(B), right). Hence, no effective STDP-mediated unlearning of the pathological connectivities takes place. In summary, the main findings are as follows:

- CR stimulation induces an overall anti-kindling of the network. HF stimulation is not able to do this.
- CR stimulation causes a segregation of the sensory input-related microcircuits. Again, HF stimulation cannot do this reliably.
- CR stimulation needs approximately 54% less stimulation current than HF stimulation. However, in fact the required stimulation current is considerably smaller in the case of CR stimulation since in the framework of our model the latter has curative, anti-kindling (i.e. long-lasting) effects. In contrast, HF stimulation has practically only acute effects and, hence, has to be delivered permanently.

In conclusion, CR stimulation results in a fast and distinct restoration of segregated sensory input-related microcircuits while using a minimal amount of stimulation.

4. Discussion

Two experimental observations inspired this modeling study. First, detailed staining studies using biotonylated dextran amine (BTA) applied to slices of the basal ganglia from healthy adult squirrel monkeys showed that the interconnections within and throughout the STN are organized into small local microcircuits (Shink *et al* 1996; Smith *et al* 1998). The neurons of the STN exert very specific excitatory effects on neighboring STN neurons and on small segregated populations of neurons of the pallidum (Shink *et al* 1996). In addition, staining of the corresponding neurons in the pallidum showed that these segregated populations are reciprocally connected at the synaptic level and form functional microcircuits (Shink *et al* 1996; Smith *et al* 1998). Shink, Smith and co-authors conclude that the failure in detecting numerous correlations between pairs of STN neurons in the healthy situation (Bergman and DeLong 1989; Nini *et al* 1995) might simply reflect the failure to detect interconnected neurons (belonging

to the same microcircuit) and does not evidence the existence of diffuse connections within and throughout the STN (Shink *et al* 1996; Smith *et al* 1998). Second, a large number of experimental results evidence that the normal dopaminergic system supports segregation of functional sub-circuits within the basal ganglia, while a loss of this segregation is a hallmark of Parkinson's disease (Bergman *et al* 1998; Pessiglione *et al* 2005). It is still a matter of debate if and how the two dominating effects of dopamine depletion—higher firing rates and bursty firing patterns resulting in the hyperactivity of the basal ganglia output structures and a loss of functional segregation in the cortico-basal-ganglia circuits—depend on each other (Pessiglione *et al* 2005).

Our mathematical model addresses this issue by, first, considering a simplified sub-structure (the STN-GPe network) of the hyperactive basal ganglia network and, second, by including the additional localized input mimicking sensory information that has to be processed by the simplified network. The striatum serves as the recipient of the sensory input from the cortex and is linked with the simplified sub-structure used in our modeling approach (Bergman *et al* 1998; Pessiglione *et al* 2005). The formation of segregated microcircuits is reflected by modifications of the synaptic connectivities, which are subject to an activity-dependent learning rule. The sensory input is of the same order as the considered uncorrelated noisy input each neuron receives. The sensory input is in particular much smaller in amplitude (approximately one magnitude) than the recurrent inhibition from the GPe in the synchronized state and the impact of electrical DBS. Initialized at the desynchronized healthy state, the weak sensory input ($A_{\text{sen}} > 0.000175$) is already capable of establishing segregated microcircuits. In contrast, the weak sensory input is not sufficient to overcome pathological synchronized activity. Increasing either the amplitude of the sensory input or the size of the sub-population affected by the sensory input results in a restoration of the segregated microcircuits. Only a significant increase of the number and size of distinct microcircuits receiving the sensory input results in both a restoration of segregated microcircuits and a long-lasting reduction of pathological synchronization.

DBS with the coordinated reset protocol is able to restore the segregated microcircuits at the same time as it effectively reduces the synchronized activity. In contrast, HF DBS has no beneficial effect on both the segregation and the reduction of pathological synchronized activity. In our modeling approach, we considered a realistic combination of inhibitory and excitatory effects of the stimulation (Benabid *et al* 2005; Hauptmann and Tass 2007). As shown in Hauptmann and Tass (2007), nearly pure excitatory mechanisms of the stimulation result in an increase of the effectiveness of HF stimulation in terms of the reduction of the pathological synchronization. However, this leads to an anti-kindling, which is, in fact, observed neither electrophysiologically (Kühn *et al* 2008) nor clinically (Temperli *et al* 2003). In our model system including sensory input, we observed similar results, namely weak HF stimulation combined with nearly pure excitatory mechanisms resulted in the restoration of the segregated activity and the reduction of the synchronized pathological activity (data not shown). With the same settings, weak CR stimulation resulted in similar results in a more efficient way (i.e. faster, more robust and with less stimulation). All together, CR stimulation proved to be very efficient and robust (i.e. effective over a huge parameter range) in restoring segregated activity and reducing pathological synchronized activity at the same time.

Our findings indicate that the sensory input might have a protective, anti-kindling effect. This is in agreement with the fact that deafferentation leads to an emergence of pathological synchronization (Weisz *et al* 2007; De Ridder *et al* 2007; Bonilha *et al* 2010), see also Nolano *et al* (2008). In our model, the sensory input has the capability to reduce pathological synchronized activity; segregated information processing can be restored and desynchronized activity can be stabilized. Furthermore, weak CR DBS empowers this mechanism and has the potential to completely restore the normal functional sub-circuits of the basal ganglia.

Acknowledgments

This study was supported by the Network of Excellence in Biosimulation (BioSim LSHB-CT-20004-005137) and by the System Biology Initiative of the Helmholtz Society.

References

Benabid A L, Chabardes S and Pollak P 2009 Deep brain stimulation of the subthalamic nucleus for the treatment of Parkinson's disease *Lancet Neurol.* **8** 67–91

Benabid A L, Pollak P, Gervason C, Hoffmann D, Gao D M, Hommel M, Perret J E and de Rougemount J 1991 Longterm suppression of tremor by chronic stimulation of ventral intermediate thalamic nucleus *Lancet* **337** 403–6

Benabid A L, Wallace B, Mitrofanis J, Xia R, Piallat B, Chabardes S and Berger F 2005 A putative generalized model of the effects and mechanism of action of high frequency electrical stimulation of the central nervous system *Acta Neurol. Belg.* **105** 149–57

Bergman H and DeLong M R 1989 Electro-physiological studies of the connections of the subthalamic nucleus and globus pallidus in behaving monkeys *Soc. Neurosci. Abstr.* **15** 902

Bergman H and Deuschl G 2007 Pathophysiology of Parkinson's disease: from clinical neurology to basic neuroscience and back *Mov. Disorders* **17** S28–40

Bergman H, Feingold A, Nini A, Raz A, Slovin H, Abeles M and Vaadia E 1998 Physiological aspects of information processing in the basal ganglia of normal and Parkinsonian primates *Trends Neurosci.* **21** 32–8

Bergman H, Wichmann T, Karmon B and DeLong M R 1994 The primate subthalamic nucleus: II. Neuronal activity in the MPTP model of Parkinsonism *J. Neurophysiol.* **72** 507–20

Beurrier C, Garcia L, Bioulac B and Hammond C 2002 Subthalamic nucleus: a clock inside basal ganglia? *Thalamus Relat. Syst.* **2** 1–8

Bi G 2002 Spatiotemporal specificity of synaptic plasticity: cellular rules and mechanisms *Biol. Cybern.* **87** 319–32

Bi G and Poo M 1998 Synaptic modifications in cultured hippocampal neurons: dependence on spike timing, synaptic strength, and postsynaptic cell type *J. Neurosci.* **18** 10464–72

Bonilha L, Edwards J C, Kinsman S L, Morgan P S, Fridriksson J, Rorden C, Rumboldt Z, Roberts D R, Eckert M A and Halford J J 2010 Extrahippocampal gray matter loss and hippocampal deafferentation in patients with temporal lobe epilepsy *Epilepsia* **51** 519–28

Brown P 2003 Oscillatory nature of human basal ganglia activity: relationship to the pathophysiology of Parkinson's disease *Mov. Disord.* **18** 357–63

Brown P, Oliviero A, Mazzone P, Insola A, Tonali P and Di Lazzaro V 2001 Dopamine dependency of oscillations between subthalamic nucleus and pallidum in Parkinson's disease *J. Neurosci.* **21** 1033–8

Brown P and Williams D 2005 Basal ganglia local field potential activity: character and functional significance in the human *Clin. Neurophysiol.* **116** 2510–9

Coffey R J 2009 Deep brain stimulation devices: a brief technical history and review *Artif. Organs* **33** 208–20

De Ridder D, De Mulder G, Verstraeten E, Sunaert S and Moller A 2007 Somatosensory cortex stimulation for deafferentation pain *Acta Neurochir. Suppl.* **97** 67–74

Deuschl G, Raethjen J, Baron R, Lindemann M, Wilms H and Krack P 2000 What do the basal ganglia do? The pathophysiology of Parkinsonian tremor: a review *J. Neurol.* **247 (Suppl. 5)** 33–48

Dolan K, Witt A, Spano M L, Neiman A and Moss F 1999 Surrogates for finding unstable periodic orbits in noisy data sets *Phys. Rev.* E **59** 5235–41

Freund H-J 2005 Long-term effects of deep brain stimulation in Parkinson's disease *Brain* **128** 2222–3

Froemke R and Dan Y 2002 Spike-timing-dependent synaptic modification induced by natural spike trains *Nature* **416** 433–8

Gale J T, Shields D C, Jain F A, Amirnovin R and Eskandar E N 2009 Subthalamic nucleus discharge patterns during movement in the normal monkey and Parkinsonian patient *Brain Res.* **1260** 15–23

Gerstner W, Kempter R, van Hemmen J L and Wagner H 1996 A neuronal learning rule for sub-millisecond temporal coding *Nature* **383** 76–8

Gillies A and Willshaw D 2004 Models of the subthalamic nucleus: the importance of intranuclear connectivity *Med. Eng. Phys.* **26** 723–32

Hairer E, Norsett S P and Wanner G 1987 *Solving Ordinary Differential Equations: I* (New York: Springer)

Hauptmann C and Mackey M 2003 Stimulus-dependent onset latency of the inhibitory recurrent activity *Biol. Cybern.* **88** 459–67

Hauptmann C, Omelchenko O, Popovych O V, Maistrenko Y and Tass P A 2007 Control of spatially patterned synchrony with multisite delayed feedback *Phys. Rev.* E **76** 066209

Hauptmann C, Popovych O and Tass P A 2005 Effectively desynchronizing deep brain stimulation based on a coordinated delayed feedback stimulation via several sites *Biol. Cybern.* **93** 463–70

Hauptmann C and Tass P A 2007 Therapeutic rewiring by means of desynchronizing brain stimulation *Biosystems* **89** 173–81

Hauptmann C and Tass P A 2009 Cumulative and after-effects of short and weak coordinated reset stimulation: a modeling study *J. Neural Eng.* **6** 016004

Hebb D O 1949 *The Organization of Behavior* (New York: Wiley)

Kepecs A, van Rossum M C W, Song S and Tagner J 2002 Spike-timing-dependent plasticity: common themes and divergent vistas *Biol. Cybern.* **87** 446–458

Kita H, Chang H T and Kitai S T 1982 The morphology of intracellularly labeled rat subthalamic neurons: a light microscopic analysis *J. Comp. Neurol.* **215** 245–57

Kühn A A *et al* 2008 High-frequency stimulation of the subthalamic nucleus suppresses oscillatory β activity in patients with Parkinson's disease in parallel with improvement in motor performance *J. Neurosci.* **28** 6165–73

Kühn A A, Kupsch A, Schneider G-H and Brown P 2006 Reduction in subthalamic 8–35 Hz oscillatory activity correlates with clinical improvement in Parkinson's disease *Eur. J. Neurosci.* **23** 1956–60

Kumar R, Lozano A M, Sime E and Lang A E 2003 Long-term follow-up of thalamic deep brain stimulation for essential and Parkinsonian tremor *Neurology* **61** 1601–4

Levy R, Ashby P, Hutchinson W D, Lang A E, Lozano A M and Dostrovsky J O 2002 Dependence of subthalamic nucleus oscillations on movement and dopamine in Parkinson's disease *Brain* **125** 1196–209

Limousin P, Speelman J, Gielen F and Janssens M 1999 Multicentre European study of thalamic stimulation in Parkinsonian and essential tremor *J. Neurol. Neurosurg. Psychiatry* **66** 289–96

Mazurek M E and Shadlen M N 2002 Limits to the temporal fidelity of cortical spike rate signals *Nat. Neurosci.* **5** 463–71

Morris C and Lecar H 1981 Voltage oscillations in the barnacle giant muscle fiber *Biophys. J.* **35** 193–213

Nini A, Feingold A, Slovin H and Bergman H 1995 Neurons in the globus pallidus do not show correlated activity in the normal monkey, but phase-locked oscillations appear in the MPTP model of parkinsonism *J. Neurophysiol.* **74** 1800–5

Nolano M, Provitera V, Estraneo A, Selim M M, Caporaso G, Stancanelli A, Saltalamacchia A M, Lanzillo B and Santoro L 2008 Sensory deficit in Parkinson's disease: evidence of a cutaneous denervation *Brain* **131** 1903–11

Pessiglione M, Guehl D, Rolland A S, Francois C, Hirsch E C, Feger J and Tremblay L 2005 Thalamic neuronal activity in dopamine-depleted primates: evidence for a loss of functional segregation within basal ganglia circuits *J. Neurosci.* **25** 1523–31

Pinsky P F and Rinzel J 1995 Synchrony measures for biological neural networks *Biol. Cybern.* **73** 129–37

Pfister J P and Gerstner W 2006 Triplets of spikes in a model of spike timing-dependent plasticity *J. Neurosci.* **26** 9673–82

Popovych O, Hauptmann C and Tass P A 2005 Effective desynchronization by nonlinear delayed feedback *Phys. Rev. Lett.* **94** 164102–5

Ranck J B 1975 Which elements are excited in electrical stimulation of mammalian central nervous system: a review *Brain Res.* **98** 417–40

Richardson K A, Gluckman B J, Weinstein S L, Glosch C E, Moon J B, Gwinn R P, Gale K and Schiff S J 2003 *In vivo* modulation of hippocampal epileptiform activity with redial electric fields *Epilepsia* **44** 768–77

Rinzel J and Ermentrout G B 1989 Analysis of neural excitability and oscillations *Methods in Neuronal Modelling: From Synapses to Networks* ed C H Koch and I Segev (Cambridge, MA: MIT Press) pp 135–69

Rodriguez-Oroz M *et al* 2005 Bilateral deep brain stimulation in Parkinson's disease: a multicentre study with 4 years follow-up *Brain* **128** 2240–9

Shen K, Zhu Z, Munhall A and Johnson S W 2003 Synaptic plasticity in rat subthalamic nucleus induced by high-frequency stimulation *Synapse* **50** 314–9

Shen K and Johnson S W 2006 Subthalamic stimulation evokes complex EPSCs in the rat substantia nigra pars reticulata *in vitro J. Physiol.* **573** 697–709

Shink E, Bevan M D, Bolam J P and Smith Y 1996 The subthalamic nucleus and the external pallidum: two tightly interconnected structures that control the output of the basal ganglia in the monkey *Neurosci.* **73** 335–57

Silberstein P *et al* 2003 There is a difference in patterning of globus pallidus local field potentials between PD and dystonia *Brain* **126** 2597–608

Silberstein P, Oliviero A, Di Lazzaro V, Insola A, Mazzone P and Brown P 2005 Oscillatory pallidal local field potential activity inversely correlates with limb dyskinesias in Parkinson's disease *Exp. Neurol.* **194** 523–9

Smith Y, Bevan M D, Shink E and Bolam J P 1998 Microcircuitry of the direct and indirect pathways of the basal ganglia *Neurosci.* **86** 353–87

Smirnov D A, Barnikol U B, Barnikol T T, Bezruchko B P, Hauptmann C, Bührle C, Maarouf M, Sturm V, Freund H J and Tass P A 2008 The generation of Parkinsonian tremor as revealed by directional coupling analysis *Europhys. Lett.* **83** 20003

Svirskis G and Rinzel J 2000 Influence of temporal correlation of synaptic input on the rate and variability of firing in neurons *Biophys. J.* **79** 629–37

Stevens C F and Zador A M 1998 Input synchrony and the irregular firing of cortical neurons *Nature Neurosci.* **1** 210–7

Tass P A 1999 *Phase Resetting in Medicine and Biology* (Berlin: Springer)

Tass P A 2003 A model of desynchronizing deep brain stimulation with a demand-controlled coordinated reset of neural subpopulations *Biol. Cybern.* **89** 81–8

Tass P A and Majtanik M 2006 Long-term anti-kindling effects of desynchronizing brain stimulation: A theoretical study *Biol. Cybern.* **94** 58–66

Tass P A, Hauptmann C and Popovych O V 2006 Development of therapeutic brain stimulation techniques with methods from nonlinear dynamics and statistical physics *Int. J. Bifurcation Chaos* **16** 1889–911

Tass P A, Silchenko A N, Hauptmann C, Barnikol U B and Speckmann E J 2009 Long-lasting desynchronization in rat hippocampal slice induced by coordinated reset stimulation *Phys. Rev.* E **80** 011902

Temperli P, Ghika J, Villemure J G, Burkhard P R, Bogousslavsky J and Vingerhoets F J 2003 How do Parkinsonian signs return after discontinuation of subthalamic DBS? *Neurology* **60** 78–81

Terman D, Rubin J E, Yew A C and Wilson C J 2002 Activity patterns in a model for the subthalamopallidal network of the basal ganglia *J. Neurosci.* **22** 2963–76

Volkmann J 2004 Deep brain stimulation for the treatment of Parkinson's disease *J. Clin. Neurophysiol.* **21** 6–17

van Vreeswijk C and Sompolinsky H 1996 Choas in neuronal networks with balanced excitatory and inhibitory activity *Science* **274** 1724–6

Weisz N, Mueller S, Schlee W, Dohrmann K, Hartmann T and Elbert T 2007 The neural code of auditory phantom perception *J. Neurosci.* **27** 1476

Wichmann T, Bergman H, Starr P A, Subramanian T, Watts R L and DeLong M R 1999 Comparison of MPTP-induced changes in spontaneous neuronal discharge in the internal pallidal segment and in the substantia nigra pars reticulata in primates *Exp. Brain Res.* **125** 397–409

Wittenberg G M and Wang S S H 2006 Malleability of spike-timing-dependent plasticity at the CA3-cA1 synapse *J. Neurosci.* **26** 6610–7